

REPORT DOCUMENTATION PAGE

1a. REPORT SECURITY CLASSIFICATION UNCLASSIFIED		1b. RESTRICTIVE MARKINGS	
2a. SECURITY CLASSIFICATION AUTHORITY MAY 24 1988		3. DISTRIBUTION/AVAILABILITY OF REPORT Approved for public release; distribution is unlimited.	
AD-A193 683 RH		5. MONITORING ORGANIZATION REPORT NUMBER(S)	
6a. NAME OF PERFORMING ORGANIZATION Naval Ocean Systems Center		6b. OFFICE SYMBOL (if applicable) NOSC	
7a. NAME OF MONITORING ORGANIZATION Naval Ocean Systems Center		7b. ADDRESS (City, State and ZIP Code) San Diego, California 92152-5000	
8a. ADDRESS (City, State and ZIP Code) San Diego, California 92152-5000		8b. OFFICE SYMBOL (if applicable) NOSC	
9. PROCUREMENT INSTRUMENT IDENTIFICATION NUMBER		10. SOURCE OF FUNDING NUMBERS	
8a. NAME OF FUNDING/SPONSORING ORGANIZATION Naval Ocean Systems Center		PROGRAM ELEMENT NO. 62759N	
8b. ADDRESS (City, State and ZIP Code) San Diego, California 92152-5000		PROJECT NO. SXB3	
		TASK NO. RW59551	
		AGENCY ACCESSION NO. DN888 715	
11. TITLE (Include Security Classification) IR SKY RADIANCE DISTRIBUTIONS IN THE MARINE BOUNDARY LAYER			
12. PERSONAL AUTHOR(S) D.B. Law, et al.			
13a. TYPE OF REPORT Professional paper		13b. TIME COVERED FROM Apr 1986 TO Apr 1986	
		14. DATE OF REPORT (Year, Month, Day) April 1986	
15. PAGE COUNT			
16. SUPPLEMENTARY NOTATION			
17. COSAT CODES		18. SUBJECT TERMS (Continue on reverse if necessary and identify by block number)	
FIELD	GROUP	SUB-GROUP	electromagnetic atmospheric physics
			electro-optics
			countermeasures
19. ABSTRACT (Continue on reverse if necessary and identify by block number) Infrared optical properties of the marine boundary layer are basic in the performance of thermal imaging systems, such as forward looking infrared (FLIR) sensors, over the ocean. To aid in evaluating the performance of these sensors, spatial distributions of infrared sky radiance in the 3-5 μm mid-wavelength infrared (MWIR) and 8-12 μm long wavelength infrared (LWIR) spectral bands were measured simultaneously at low elevation angles above the sea surface. Calibrated AGA, Model 780, dual scanning systems functioned as imaging infrared radiometers. Infrared sky radiance and meteorological parameters were recorded concurrently in a series of four data sets during one diurnal cycle, starting 15 April 1986 at 1500 Pacific Standard Time (PST) and ending 16 April 1986 at 1730 PST. Radiosondes were released from the deck of the USS Poinsett, about 7.6 m above the ocean, at a range of 5 km due west of the coastal sensor site at Naval Ocean Systems Center, San Diego, CA. Wind speed, direction, sea temperature, and cloud conditions were also recorded on board the ship. Sequential images of radiance distributions provided control data for monitoring the stability or variability of atmospheric conditions throughout the time for radiosonde ascent to about 6 km altitude. Measured IR sky radiance distributions were compared with corresponding clear-sky radiance using the LOWTRAN 6 computer code. Cloud radiance and scattered solar radiation restricted the comparison to elevations close to the optical horizon where aerosol attenuation would be greatest. Infrared aerosol transmittance was inferred from the ratio of measured radiance to calculated clear-sky radiance along the horizon line-of-sight (LOS). Equivalent temperatures for blackbody radiance at the horizon were either less than or equal to the ambient air temperature near the sea surface, except when the MWIR band included scattered solar radiation; consequently, only the LWIR band could be used to infer aerosol transmittance reliably.			
20. DISTRIBUTION/AVAILABILITY OF ABSTRACT <input type="checkbox"/> UNCLASSIFIED/UNLIMITED <input checked="" type="checkbox"/> SAME AS RPT <input type="checkbox"/> DTIC USERS			
21. ABSTRACT SECURITY CLASSIFICATION UNCLASSIFIED		22a. NAME OF RESPONSIBLE INDIVIDUAL D.B. Law	
22b. TELEPHONE (Include Area Code) (619) 553-2630		22c. OFFICE SYMBOL Code 754	

19. ABSTRACT (Continued)

Radiance along the optical horizon originated mainly in the lowest 100 m of the atmosphere; therefore, reasonably accurate horizon radiance or transmittance predictions could be made from meteorological data within this low altitude. These results indicate that a LWIR aerosol transmissometer could be developed by computing the ratio of measured horizon sky radiance to calculated clear-sky radiance using local ambient meteorological data.



Accession For	
NTIS GRA&I	<input checked="" type="checkbox"/>
DTIC TAB	<input type="checkbox"/>
Unannounced	<input type="checkbox"/>
Justification	
By _____	
Distribution/	
Availability Codes	
Dist	Avail and/or Special
A-1	

IR sky radiance distributions in the marine boundary layer

William J. Schade

Alcoa Defense Systems, Inc.
16761 Via Del Campo Court
San Diego, CA 92128

David B. Law

Naval Ocean Systems Center
San Diego, CA 92152-5000

ABSTRACT

Infrared optical properties of the marine boundary layer are basic in the performance of thermal imaging systems, such as forward looking infrared (FLIR) sensors, over the ocean. To aid in evaluating the performance of these sensors, spatial distributions of infrared sky radiance in the 3- 5 μm mid-wavelength infrared (MWIR) and 8 - 12 μm long wavelength infrared (LWIR) spectral bands were measured simultaneously at low elevation angles above the sea surface. Calibrated AGA, Model 780, dual scanning systems functioned as imaging infrared radiometers. Infrared sky radiance and meteorological parameters were recorded concurrently in a series of four data sets during one diurnal cycle starting 15 April 1986 at 1500 Pacific Standard Time (PST) and ending 16 April 1986 at 1730 PST. Radiosondes were released from the deck of the USS POINT LOMA, about 7.6 m above the ocean, at a range of 5 km due west of the coastal sensor site at Naval Ocean Systems Center, San Diego, CA. Wind speed, direction, sea temperature, and cloud conditions were also recorded on board the ship. Sequential images of radiance distributions provided control data for monitoring the stability or variability of atmospheric conditions throughout the time for radiosonde ascent to about 6 km altitude.

Measured IR sky radiance distributions were compared with corresponding clear-sky radiance using the LOWTRAN 6 computer code. Cloud radiance and scattered solar radiation restricted the comparison to elevations close to the optical horizon where aerosol attenuation would be greatest.

Infrared aerosol transmittance was inferred from the ratio of measured radiance to calculated clear-sky radiance along the horizon line of sight (LOS). Equivalent temperatures for blackbody radiance at the horizon were either less than or equal to the ambient air temperature near the sea surface, except when the MWIR band included scattered solar radiation; consequently, only the LWIR band could be used to infer aerosol transmittance reliably.

Radiance along the optical horizon originated mainly in the lowest 100 m of the atmosphere; therefore, reasonably accurate horizon radiance or transmittance predictions could be made from meteorological data within this low altitude. These results indicate that a LWIR aerosol transmissometer could be developed by computing the ratio of measured horizon sky radiance to calculated clear-sky radiance using local ambient meteorological data.

1. INTRODUCTION

The effects of aerosols on the propagation of infrared radiation through the marine boundary layer are basic in the use of both active and passive remote sensing systems over the ocean. The extent to which these effects can be evaluated and modeled depends largely on the methods for characterizing the atmospheric constituents along the optical path.

Current methods for measuring particle sizes and concentrations are limited to local sampling volumes at the sensor site which are not characteristic of extended path lengths. Lidar measurements have been used to compute total volume extinction coefficients as a function of range; however, lidar data are generally acquired at sequential intervals along different directions between which the meteorological conditions could change without notice. Additional uncertainties arise when lidar data at one wavelength are applied to other spectral regions.

An alternative method for inferring the effects of aerosols on atmospheric transmittance is describe in this paper. Spatial distributions of infrared sky radiance in the 3- to 5- μm mid-wavelength infrared (MWIR) and 8- to 12- μm long

wavelength infrared (LWIR) spectral bands were measured at low elevation angles above the sea surface. These distributions represent the integrated radiance propagated along contiguous optical paths through the entire atmosphere within the field of view (FOV) of the calibrated thermal imaging sensor. Since the FOV of the AGA Thermovision 780 is scanned in 40 ms, the data for each distribution are almost simultaneous.

The extent to which the measured radiance differs from the corresponding clear-sky radiance can be used to imply the effective transmittance. The clear-sky radiance was computed with the LOWTRAN 6 computer code using radiosonde measurements of meteorological parameters concurrent with the measured radiance over the ocean.¹ This technique offers a viable method for evaluating the total aerosol effect through the entire marine boundary layer by remote sensing.

The data were obtained during one diurnal cycle starting 15 April 1986 at 1500 Pacific Standard Time (PST) and ending 16 April 1986 at 1730 PST. The sensor LOS was directed along an azimuth of 270 degrees true radial from NOSC, building T323, located at 32.699 degrees N latitude, 117.253 degrees W longitude, at a height of 33 m above sea level.

Radiosondes were released from the deck of the USS POINT LOMA (AGDS 2) about 7.6 m above the sea surface at a range of 5 km from the sensor site. Wind speed, direction, and sea temperatures were also recorded on board the ship, as well as cloud conditions. A complete description of the shipboard data is available.²

Throughout this report, clear-sky radiance refers to the atmosphere without aerosols. This corresponds to IHAZE = 0 in the LOWTRAN 6 computer code when $\tau_s = 1$ in the LOWTRAN calculations for sky radiance (where τ_s is transmittance due to scattering). This is regarded as the reference condition for comparing the respective measurements in the LWIR and MWIR spectral bands.

2. ATMOSPHERIC MEASUREMENTS

Infrared sky radiance and meteorological measurements were recorded simultaneously in a series of four data sets. Table 1 lists the dates and times for the measurements along with the solar positions. Surface meteorological measurements were made at the NOSC sensor site as well as shipboard, while the vertical profiles were measured by radiosondes released from the USS POINT LOMA. The air and sea temperatures, wind speed, and direction are also listed in table 1.

Table 1. Atmospheric measurements series for meteorological parameters.

Data Set	1	2	3	4
Date	15 Apr 86	16 Apr 86	16 Apr 86	16 Apr 86
Radiosonde Time (PST)	1945	0845	1245	1645
Solar Position (degrees)				
Azimuth	295	106	212	270
Zenith	140	49	26	71
Air Temp. (°C)	15.0	15.4	15.5	15.7
Wind Speed (knots)	10	9	20	20
Direction (degrees)	300	330	280	310
Sea Temp. (°C)	17.8	16.7	17.2	17.2

Figures 1, 2, 3, and 4 show the radiosonde measurements for temperature and relative humidity plotted with respect to altitude. These data were used in the LOWTRAN 6 computer code to calculate clear-sky radiance as a function of elevation angle above the horizon. The data in figure 1 were used to evaluate the meteorological sensitivities of the radiance calculations. This set presents the nighttime data for a well-defined cloud-top boundary and an adiabatic lapse rate of 9.8°C in the first kilometer above sea level.

The uncertainty in relative humidity is estimated to be 5 percent, which provides a better approximation to the water vapor density than any of the standard model atmospheres. The sensitivity of the radiance calculations to this uncertainty in humidity was examined by incrementing the relative humidity profile ± 5 percent while keeping the temperature profile unchanged from the measured values. Similarly, the sensitivity to the temperature uncertainty of ± 0.5 °C was evaluated for the observed relative humidity profile of figure 1.

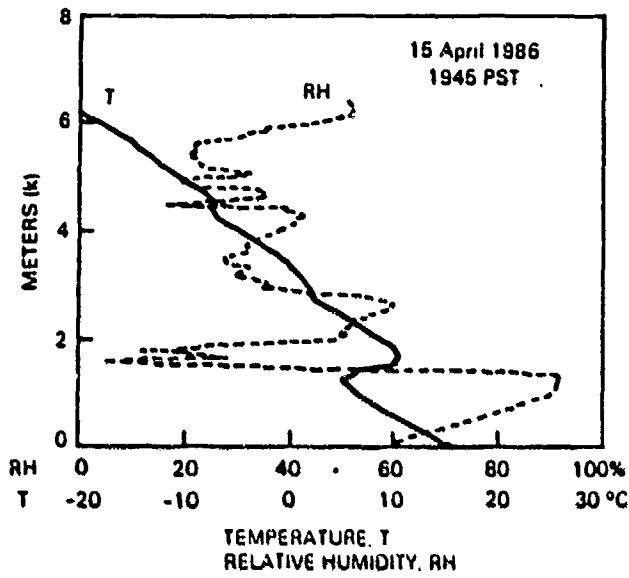


Figure 1. Radiosonde measurements for data set 1.

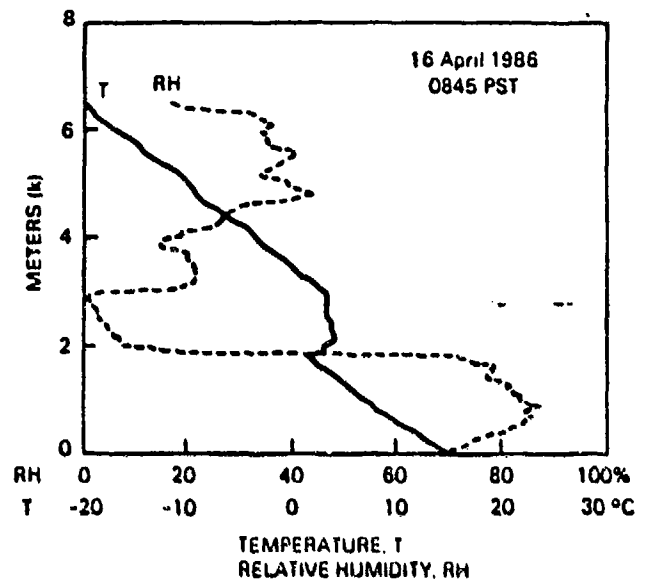


Figure 2. Radiosonde measurements for data set 2.

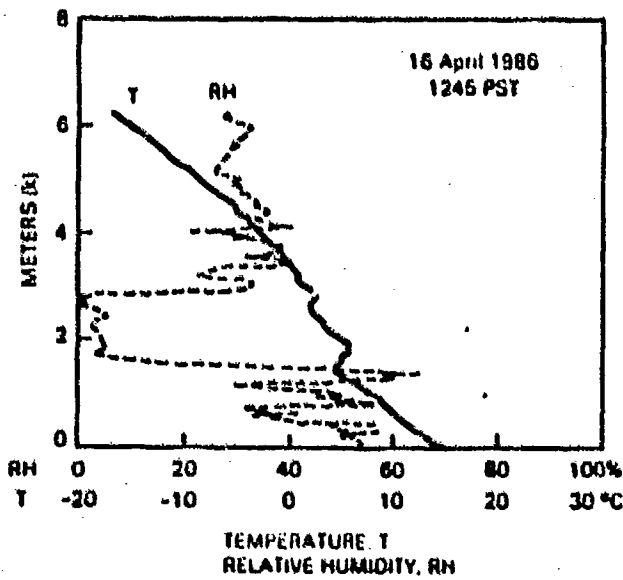


Figure 3. Radiosonde measurements for data set 3.

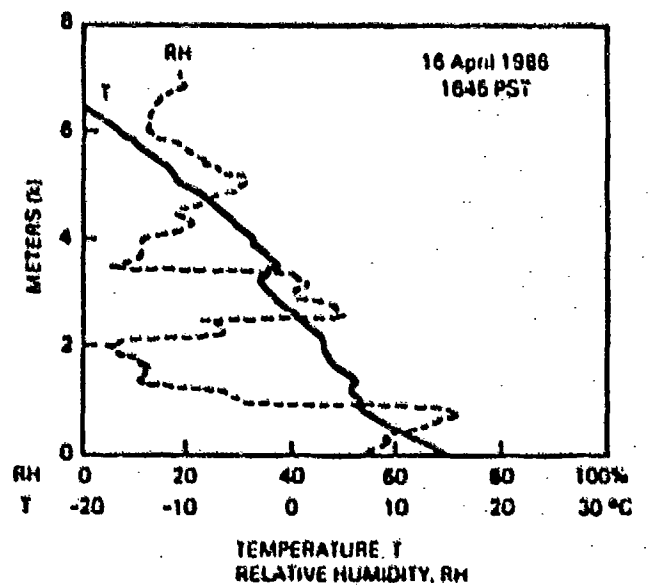


Figure 4. Radiosonde measurements for data set 4.

Figure 5 shows the comparative effects of deviations in temperature and relative humidity. The calculated clear-sky radiance, for IHAZE = 0, is plotted as a function of elevation angle. Radiance discrepancies resulting from relative humidity errors are less than those resulting from temperature errors throughout the range of elevation from 0 to 2 degrees. For elevation less than 0.5 degree, the effects of errors in relative humidity are negligible compared with those in temperature. A temperature error of $\pm 0.5^\circ\text{C}$ changes the radiance by about $\pm 0.033 \text{ mw}/(\text{cm}^2 \cdot \text{str})$ in the LWIR band and about $\pm 0.0033 \text{ mw}/(\text{cm}^2 \cdot \text{str})$ in the MWIR band.

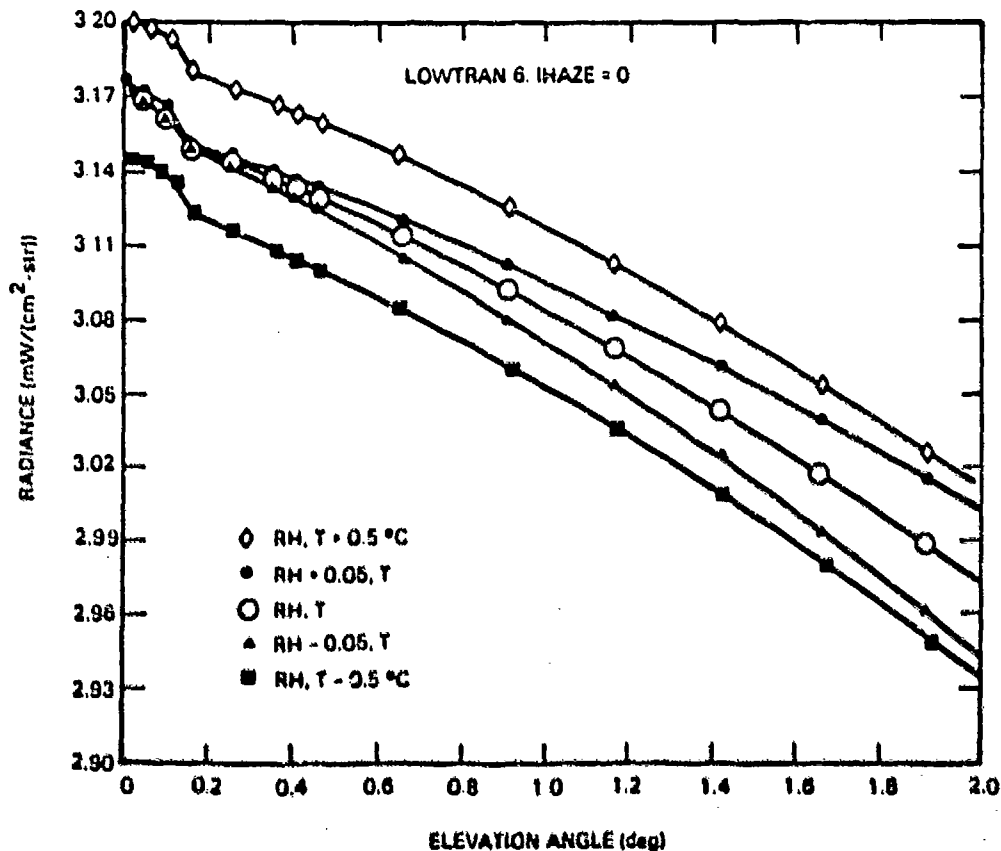


Figure 5. Calculated clear-sky distributions of LWIR radiance above the horizon for comparative errors in temperature ($T \pm 0.5^\circ\text{C}$) and relative humidity ($\text{RH} \pm .05$) profiles.

Sky radiance data were acquired in the 3.5- to 5.5- μm and 8- to 12- μm spectral bands simultaneously with the AGA 780 dual scanning systems functioning as imaging radiometers. The operational characteristics of the sensor systems are listed in table 2. The analog video signals in the 3- by 3-degree FOV are interfaced through a Datalink analog-to-digital converter to a digital image processor. The format of the digital display is 128 by 128 pixels with 8-bit resolution. The minimum detectable temperature difference (MDTD) between adjacent instantaneous fields of view (IFOVs) is 0.1°C .

The total system response for each spectral band is calibrated in isotherms which represent the video signal amplitudes for radiation from a blackbody at a measured temperature and close range. Sets of conversion curves relating isotherms to object temperatures (with emissivity = 1) are obtained with the expression

$$I = C1/(C3 \cdot \exp(C2/T) - 1), \quad (1)$$

where T is the blackbody temperature in degrees Kelvin. The constants C1, C2, and C3 are derived for the calibration source at several different temperatures.

Table 2. AGA Thermovision 780 dual scanning systems operational characteristics.

Scanner	SWIR	LWIR	Both
Spectral Band: μm	3.5 to 5.5	8 to 12	
Detector: 1 each	InSb	HgCdTe	
Temperature: $^{\circ}\text{K}$			77
FOV (az by el): degrees			3 by 3
IFOV (ax by el): mrad			1.2 by 0.9
Telescope Objective			
Diameter: cm			10.6
Focal Ratio			1.8
FOV Scan Mode			
Horiz. Line Time: ms			0.4
Vert. Field Time: ms			40
Field Rate: Hz			25
Frame Rate: Hz			6.25
IFOV dwell: μs			5.3
Signal Processing: AC + DC Restored			
MDTD: $^{\circ}\text{C}/\text{IFOV}$			0.1
Temp. Range: $^{\circ}\text{C}$			-20 to 1000

The original image is analyzed with the microcomputer by assigning the equivalent blackbody temperature to the corresponding isotherm value for selected pixels in the FOV, through the transposition of equation 1,

$$T = C2/\ln u, \quad (2)$$

where

$$u = ((C1/I) + 1)/C3.$$

Radiance values are computed for each blackbody temperature through the integration of Planck's equation for the appropriate spectral band. The final form of the equation for radiance as a function of isotherms is

$$L(\text{SB}, T) = a \cdot I(T) - b, \quad (3)$$

where SB is the spectral band, a is the slope, b is the intercept, and I(T) is a nonlinear function of T in equation 1. The constants for converting isotherms to radiance in equation 3 are listed in table 3 for each spectral band, as well as the calibration source characteristics.

Table 3. Calibration constants for converting isotherms to radiance.

Scanner	SWIR	LWIR	Both
C1: Isotherms	383140.4	1514.4	
C2: $^{\circ}\text{K}$	2945.0	1294.2	
C3: dimensionless	1.0	0.503	
a: $\text{mw}/(\text{cm}^2 \cdot \text{str} \cdot \text{isotherm})$	$9.695 \cdot 10^{-6}$	$1.002 \cdot 10^{-4}$	
b: $\text{mw}/\text{cm}^2 \cdot \text{str}$	$1.556 \cdot 10^{-5}$	$1.002 \cdot 10^{-4}$	
Calibration Source			
Distance: m			3.0
Emissivity: ± 0.01			0.98
Temperature: $\pm 0.1^{\circ}\text{C}$			15-100

The main source of uncertainty in the conversion to radiance is in the isotherm values for the video signal amplitudes. Isotherms are calculated with the microcomputer to within ± 0.1 , so that the temperature of the calibration source is

reproduced within $\pm 0.2^\circ\text{C}$. This uncertainty in the temperature causes a radiance error of $\pm 0.01 \text{ mW}/(\text{cm}^2 \cdot \text{str})$ in the LWIR band, and $\pm 0.001 \text{ mW}/(\text{cm}^2 \cdot \text{str})$ in the SWIR band.

In each of the four data sets, both infrared sensor systems were referenced to a calibration source at ambient air temperature within 1 hour prior to the radiosonde ascent. Thermal images of sky radiance were recorded continuously on analog video tape and sequentially on digital diskette during 1 hour preceding and following the radiosonde measurements. These data provide an unambiguous verification of either the stability or variability of the sky radiance distributions during meteorological measurements. No measurable changes were observed during each of the data sets reported here, except for temporal variations in cloudiness.

3. RADIANCE DISTRIBUTIONS

Figure 6 shows the four LWIR radiance distributions as a function of elevation angle above the optical horizon. Zero degrees elevation corresponds to the IFOV tangent to the sea surface where the radiance is maximum. The elevation IFOV angular subtense of 0.05 degree is shown in the figure as well as the radiance uncertainty corresponding to a temperature deviation of $\text{TD} = \pm 0.2^\circ\text{C}$.

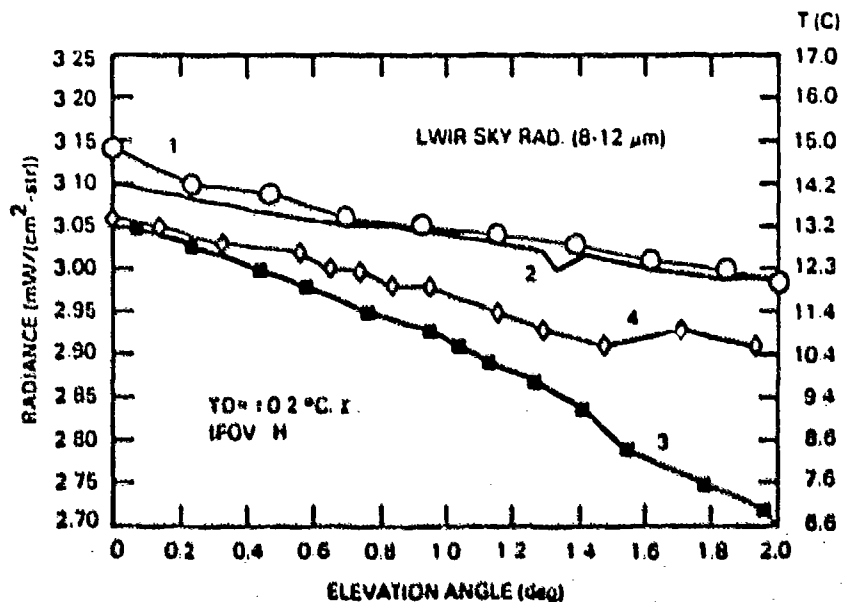


Figure 6. LWIR sky radiance distributions above the horizon; plot 1: 15 April 86, 1945 PST; plot 2: 16 April 86, 0845 PST; plot 3: 16 April 86, 1245 PST; plot 4: 16 April 86, 1645 PST.

Cloud radiance contributions are apparent at elevations greater than 0.4 degree. Scattered solar radiation from clouds is especially notable in data set 4, when the sun is about 20 degrees above the sensor LOS.

The radiances for data sets 3 and 4 are equal within the measurement uncertainty, for low elevations between 0 and 0.3 degree; however, the solar zenith angle changed from 26 degrees in data set 3 to 71 degrees in data set 4. These conditions imply that aerosol scattering of solar radiation is negligible in the LWIR band since the meteorological parameters are nearly the same for these two data sets as shown in figures 3 and 4.

Figure 7 shows the MWIR sky radiance distributions. These four plots are concurrent with those of the LWIR data. On the radiance scale used in figure 7, plots 1, 2, and 3 are approximately equal, within the temperature deviation $\text{TD} = \pm 0.2^\circ\text{C}$. Plot number 4 shows a very large increase in radiance resulting from scattered solar radiation in the clouds and lower atmospheric levels. The equivalent blackbody temperature scales are shown along the ordinates on the right of figures 6 and 7.

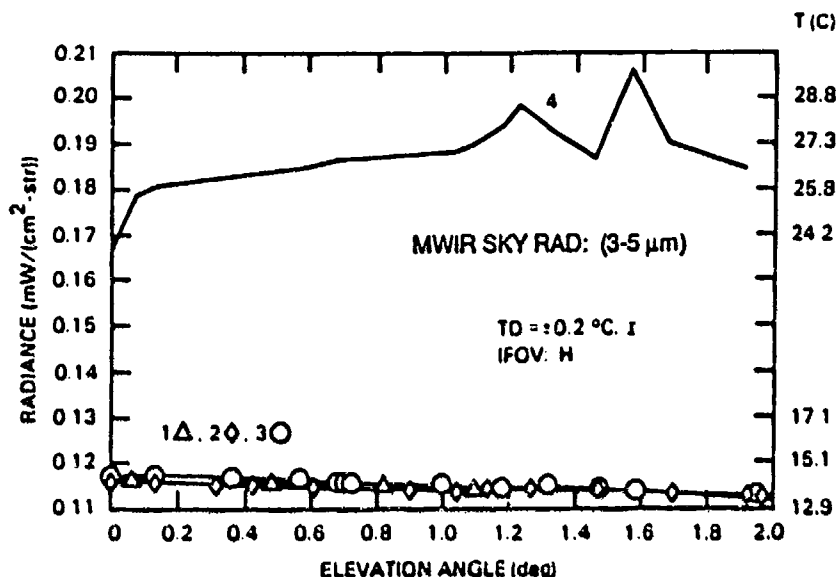


Figure 7. MWIR sky radiance distributions above the horizon and coincident with the LWIR distributions.

Figures 8 and 9 compare the observed radiance distributions and the corresponding calculated clear-sky radiances. Figures 8a, b, c, and d show the distributions for the LWIR band, and figures 9a, b, c and d show those for the MWIR band.

The clear-sky radiances were calculated using atmospheric models with 30 layers in the LOWTRAN 6 computer code. The meteorological entries were provided by the radiosonde data. The concentrations of uniformly mixed gases and ozone were those in the 1962 U.S. Standard model atmosphere.

The importance of the humidity and temperature lapse rates in calculating sky radiance distributions in the boundary layer was noted previously.³ Accordingly, the first kilometer above sea level was divided into 10 levels with about 1°C increments for each 100 m between levels. The remaining atmosphere was divided into 20 levels between 1 and 5.5 km. The radiosonde data terminated at about 6 km.

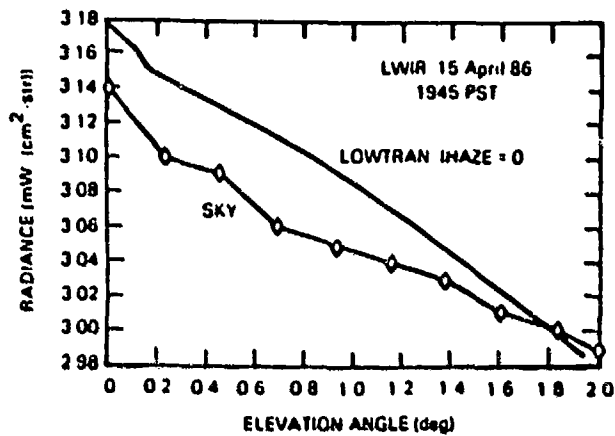
The LOWTRAN expression for calculating atmospheric radiance (Kneizys et al., 1980) is

$$L(SB) = \sum_{i=1}^{N-1} (\ln(i) - \ln(i+1)) B\left(SB, \frac{T(i) + T(i+1)}{2}\right) \left(\frac{\ln(i) + \ln(i+1)}{2}\right) + B(SB, T(b)) \ln \quad (4)$$

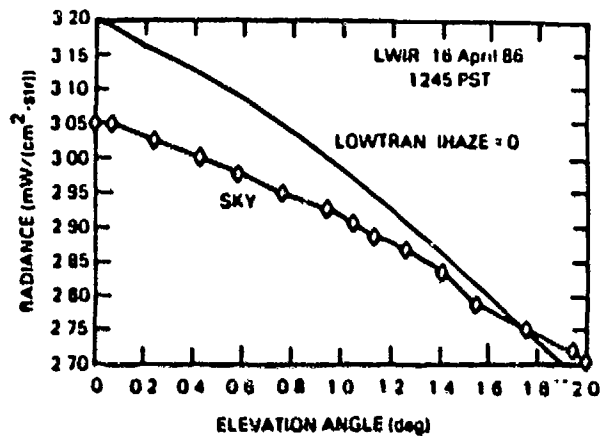
where the summation along a specified LOS is over (N - 1) isothermal layers at temperatures T (i), and

- SB = spectral band: 3 to 5 μm or 8 to 12 μm
- ln = band average transmittance due to absorption,
- ln = band average transmittance due to single scattering,
- ln = band average transmittance from sensor to cloud boundary,
- B(SB,T) = Planck blackbody function for a spectral band and average temperature T of an atmospheric layer.

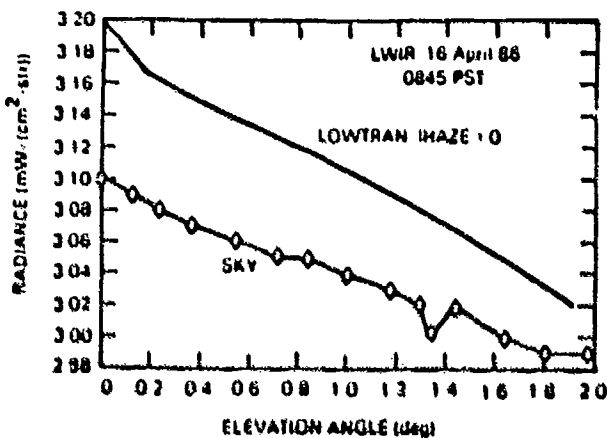
To avoid the effects of cloud radiance, the comparison of observed-to-calculated radiance is restricted to the horizon LOS where the atmospheric optical depth and aerosol attenuation are greatest. Along zero elevation, the LWIR molecular (absorption) transmittance, ln, is less than 1×10^{-4} through the 137-km horizontal optical path to the cloud base. With a cloud-base temperature of 6.8°C, the maximum LWIR cloud radiance is 2.7 mW/(cm² - sr), which becomes negligible at the sensor aperture.



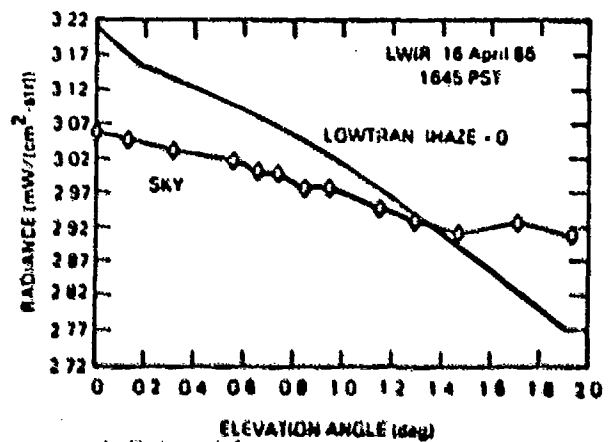
a. Data set 1



c. Data set 3



b. Data set 2



d. Data set 4

Figure 8. Comparison of measured LWIR sky radiance distributions with calculated clear-sky radiance from LOWTRAN 6: IHAZE = 0.

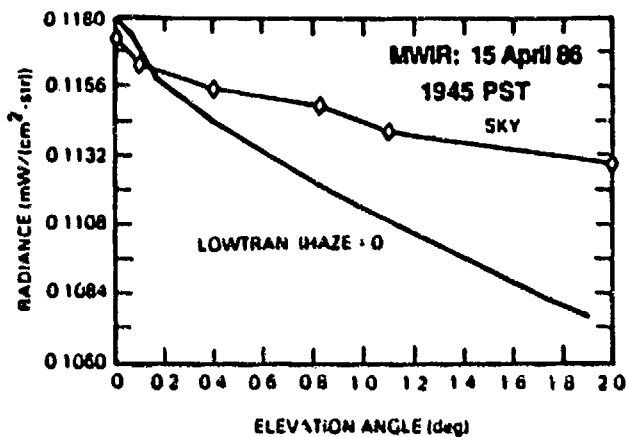
For calculation of clear-sky radiance, $\epsilon_s = 1$ for all atmospheric layers. Along the horizon LOS, the sky radiance originates predominantly in the lowest layer which approximates a horizontally homogeneous atmosphere about 100 m high. This condition is clearly evident in table 4 which lists the LWIR radiance and band average absorption transmittance, μ_a , for ranges along the horizon LOS to five levels in the first nine atmospheric layers. Over 99 percent of the clear-sky radiance along the horizon LOS is attributable to the lowest 100 m of the atmosphere. Within this lowest layer, equation 4 reduces to

$$L(SB,1) = (1 - \mu_a(1)) B(SB,T(1)). \quad (5)$$

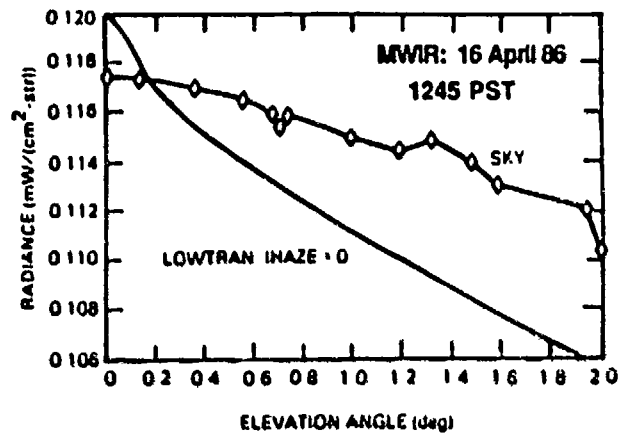
From table 4, $\mu_a(1) \cong .004$, so the emissivity of the lowest layer, $\epsilon(1) = 1 - \mu_a(1)$, is very close to unity through application of Kirchoff's law. Thus, the clear-sky radiance in the lowest layer should equal the blackbody radiance at ambient air temperature as reported previously.^{4,5} The effects of aerosols on infrared sky radiance can be inferred from equations 4 and 5 by including the transmittance due to scattering. The transmitted radiance along the horizon LOS then becomes

$$L(SB) = L(SB) \cdot \epsilon_s. \quad (6)$$

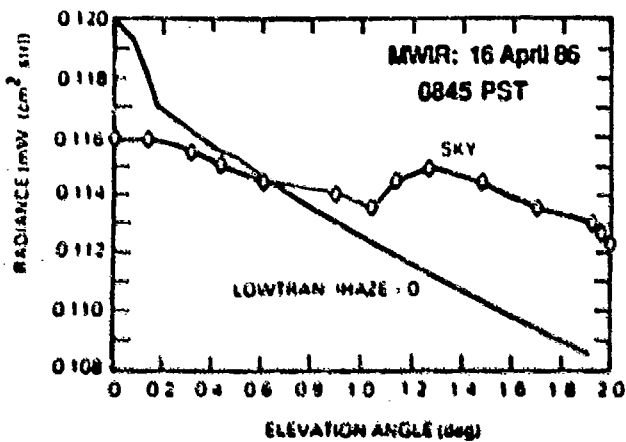
where $L(SB)$ is the clear-sky radiance given by equation 5 extended to all 30 layers.



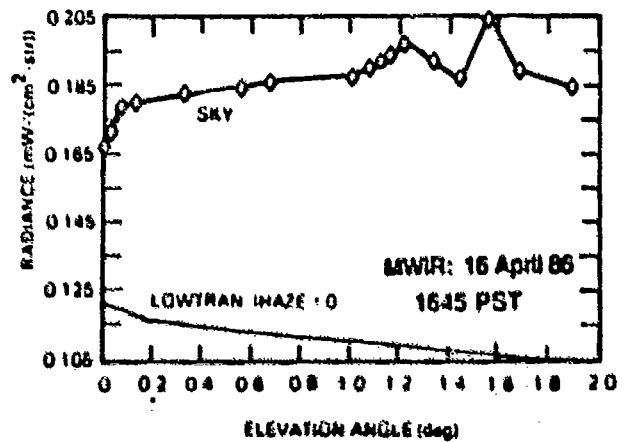
a. Data set 1



c. Data set 3



b. Data set 2



d. Data set 4

Figure 9. Comparison of measured MWR sky radiance distributions with calculated clear-sky radiance from LOWTRAN 6; IHAZE = 0.

Table 4. LWIR radiance and transmittance along the horizon LOS for data set 1, LOWTRAN 6; IHAZE = 0

Layers	Altitude to top (m)	Range to top (km)	Radiance $mW/cm^2 \cdot sr$	% Max Radiance	Average Transmittance
1	143	67	3.163	99.7	0.0036
2	263	84	3.171	99.9	0.0011
3	383	97	3.172	99.9	0.0004
5	575	114	3.173	100	0.0001
9	1016	145	3.173	100	0.0000

Absorption by aerosols would tend to bring the emissivity of the atmosphere closer to unity through τ_a , which would change by less than 1 percent from the transmittance due to molecular absorption for clear-sky conditions. Molecular scattering, however, is negligible in the spectral range of 3 to 12 μm , so τ_a can be assigned primarily to aerosols. Thus, the scattering transmittance, τ_s , was calculated with equation 6 using the measured sky radiance for L (SB)', which represents the transmitted radiance along the optical LOS from the sensor receiving aperture to space.

A summary of the horizon sky temperatures and aerosol transmittance is presented in table 5 for each set of radiosonde data. The temperatures corresponding to the measured horizon sky radiance and calculated clear-sky radiance are listed for the LWIR and SWIR bands. The radiosonde base temperatures and sensor (local) air temperatures are also given. Within each data set, the temperature differences are less than the uncertainties in the measurements except for the equivalent temperatures of the measured sky radiance. Reduced equivalent temperatures in the LWIR band correspond to aerosol scattering loss in radiance, while the increased temperature in the MWIR indicates additional radiance from scattered solar radiation in data set 4.

The calculated aerosol transmittances for both infrared bands are listed in table 5. The LWIR values show a slight aerosol effect in data sets 3 and 4, but the MWIR values are inconsistent. Although the values for both infrared bands agree in the nighttime and morning runs when the aerosols were negligible, the MWIR band cannot be used reliably to indicate aerosol attenuation when scattered solar radiation must be included. As noted above, the horizon LWIR values were unaffected by solar scattering for zenith angles from 26 to 71 degrees.

Table 5. Horizon sky temperature and aerosol transmittance.

Data Set	1	2	3	4
Date	15 Apr 86	16 Apr 86	16 Apr 86	16 Apr 86
Time (PST)	1945	0845	1245	1645
RAOB Base ($\pm 0.5^\circ\text{C}$)	15.0	15.4	15.5	15.7
Local Air ($\pm 0.3^\circ\text{C}$)	14.6	15.2	15.1	15.8
LOWTRAN 6: Clear-Sky				
MWIR	14.6	15.1	15.1	15.2
LWIR	15.4	15.9	15.9	16.1
Measured Sky ($\pm 0.2^\circ\text{C}$)				
MWIR	14.5	14.2	14.5	23.7
LWIR	14.7	14.2	13.1	13.4
Aerosol Transmittance				
MWIR	.99	.97	.98	1.38
LWIR	.99	.97	.95	.95

4. CONCLUSIONS

The AGA Thermovision 780 dual scanning system was used to measure infrared sky radiance distributions in the MWIR and LWIR spectral bands simultaneously. Sequential images of radiance distributions provided control data for monitoring the stability or variability of atmospheric conditions throughout the concurrent time for radiosonde ascent.

Measured infrared sky radiance distributions were compared with the corresponding clear-sky radiance using the LOWTRAN 6 computer code. The presence of cloud radiance and scattered solar radiation restricted the comparison to elevations close to the horizon where aerosol attenuation would be greatest.

The infrared aerosol transmittance was inferred from the ratio of measured radiance to calculated clear-sky radiance along the horizon LOS. The equivalent temperatures for blackbody radiance at the horizon were either less than or equal to the ambient air temperature near the sea surface, except when the MWIR band included scattered solar radiation. Because of this, only the LWIR band can be used to infer aerosol transmittance reliably.

The radiance along the horizon LOS originates predominantly in the lowest 100 m of the atmosphere; therefore, reasonably accurate horizon radiance or transmittance predictions could be made from meteorological data within this low altitude. These conclusions suggest that a LWIR aerosol transmissometer could be developed by computing the ratio of the

measured horizon sky radiance to the calculated clear-sky radiance using the local ambient meteorological data. Such a point-measuring system would only require a calibrated nonimaging radiometer to record the radiance along the horizon LOS.

5. ACKNOWLEDGMENTS

The authors gratefully acknowledge the radiosonde data provided by H.G. Hughes and R.A. Paulus.

6. REFERENCES

1. Kneizys, F.X., E.P. Shettle, W.O. Gallery, J.H. Chetwynd, Jr., L.W. Abreu, J.E.A. Selby, R.W. Fenn, and R.A. McClatchey (1983). "Atmospheric Transmittance/Radiance: Computer Code LOWTRAN 6," Air Force Geophysics Laboratory AFGL-TR-83-0187.
2. Jensen, D.R. (1986). "Temperature Measurements of the USS Point Loma for FLIR Evaluation Studies," Naval Ocean Systems Center TD 971.
3. Ben-Shalom, A., A.D. Devir, and S.G. Lipson (1983). *Opt. Eng.* 22:460.
4. Bennett, H.E., J.M. Bennett, and M. R. Nagel (1960). "Distribution of Infrared Radiance over a Clear-Sky," *J. Opt. Soc. Am.* 50(2):100-106.
5. Bell, E.E., L. Eisner, J. Young, and R.A. Oetjen (1960). "Spectral Radiance of Sky and Terrain at Wavelengths between 1 and 20 Microns. II. Sky Measurements," *J. Opt. Soc. Am.* 50 (12):1313-1320.
6. Kneizys, F.X., E.P. Shettle, W.O. Gallery, J.H. Chetwynd, Jr., L.W. Abreu, J.E.A. Selby, R.W. Fenn, and R.A. McClatchey (1980). "Atmospheric Transmittance/Radiance: Computer Code LOWTRAN 5," Air Force Geophysics Laboratory AFGL-TR-80-0067.